

Tunable Perovskite Semiconductor $CH_3NH_3SnX_3$ (X: Cl, Br, or I) Characterized by X-ray and DTA

Koji Yamada,* Kyosuke Nakada, Yonosuke Takeuchi, Kaori Nawa, and Yohei Yamane

Department of Applied Molecular Chemistry, College of Industrial Technology, Nihon University, Izumi-cho, Narashino, Chiba 275-8575

Received March 7, 2011; E-mail: yamada.kouji@nihon-u.ac.jp

A series of perovskite halide solid solutions was synthesized and characterized by DTA and X-ray diffraction. The solid solution $CH_3NH_3SnBr_{3-x}Cl_x$ ($x = 0$–3) changes its color from red, orange, yellow to a colorless state with increasing x. Although each highest temperature phase belongs to a cubic system, a slight trigonal distortion was observed above $x = 1.0$ at room temperature. Similar continuous solid solutions with black colors were confirmed for $CH_3NH_3SnBr_{3-x}I_x$ ($x = 0$, 1, 2, and 3) keeping a cubic perovskite structure over the whole x region. On the other hand, continuous solid solutions $CH_3NH_3SnI_{3-x}Cl_x$ could not be confirmed. The solid-state static ^{1}H NMR suggested that the isotropic reorientation of the cation does not freeze even at 150 K for the perovskite having a large anionic sublattice. The characteristic changes of the color and the electric structure for these perovskites were discussed analytically on the basis of the tight-binding approach. This simple one-dimensional expression predicts that the tin(II) perovskite halide is a direct band gap semiconductor with tailorable properties.

Perovskite oxides are interesting and important materials because of their functional properties, such as electronic conductivity, ionic conductivity, ferroelectric, ferromagnetic, and catalytic properties. Although perovskite halides ABX_3 (X = F, Cl, Br, and I) are chemically and also thermally unstable compared to the oxides, a variety of functional properties similar to the oxides have been reported. Recently formability of halide perovskite ABX_3 was investigated over 186 complex halides using empirical Goldschmit's tolerance factor and the octahedral factor (r_B/r_X) including transition metals and main group metals.[1] The most well known halide perovskites having transition elements are $AMnF_3$, $AFeF_3$, and $ACuF_3$ (A: monovalent cation) in which magnetic divalent cations are included as B. On the other hand, main group elements such as Ca^{2+}, Ge^{2+}, Sn^{2+}, Pb^{2+}, Cd^{2+}, and Hg^{2+} also form perovskite halide with A^+ cation having a suitable ionic radius. Recently, metathesis syntheses of perovskite fluorides have been reported using mechanochemical activation instead of expensive equipment or high temperature.[2]

Perovskite fluorides have been studied as host materials of fluorescence[3] and as good fluoride ionic conductors.[4,5] Perovskite bromides and iodides, on the other hand, have been extensively studied for Sn(II) compounds because of their characteristic phase transitions and electronic structures. For example, successive structural phase transitions,[6–12] transport and optical properties,[13,14] preparation and characterization of thin films,[15–18] and theoretical calculations of the band structure[19–21] have been reported. A visible-light sensitizer in a photoelectrochemical cell was also studied for the Pb analog.[22] Recent ab initio calculations suggested that although the valence and conduction bands take negligible contribution from the cation A^+, the band gap can be tuned by a suitable choice of cation.[17,21] That is, the electronic properties of Sn(II) perovskite halides are strongly dependent on the dimension of the three-dimensional network of the SnX_6 octahedra. Since perovskite halides form a series of solid solutions between different halides, tunable semiconductors could also be synthesized controlling their compositions. This is the most pronounced feature of the perovskite halide compared to the oxide.

Figure 1 shows a photograph for a series of solid solutions $CH_3NH_3SnBr_{3-x}Cl_x$ precipitated from the relevant solutions. Their colors change continuously from a red to a colorless state with increasing x. Their solutions after heating, however, show no characteristic colors, since the colors arise purely from their band structures.

In this study we evaluated the possibility of the new solid solutions between perovskite halides of Sn(II), i.e.,

Figure 1. A photograph of a series of $CH_3NH_3SnBr_{3-x}Cl_x$ precipitations from the relevant solutions ($x = 3.0$, 2.0, 1.0, 0.5, and 0.0 from the left). After heating these solutions, they change to colorless solutions.

Published on the web August 27, 2011; doi:10.1246/bcsj.20110075

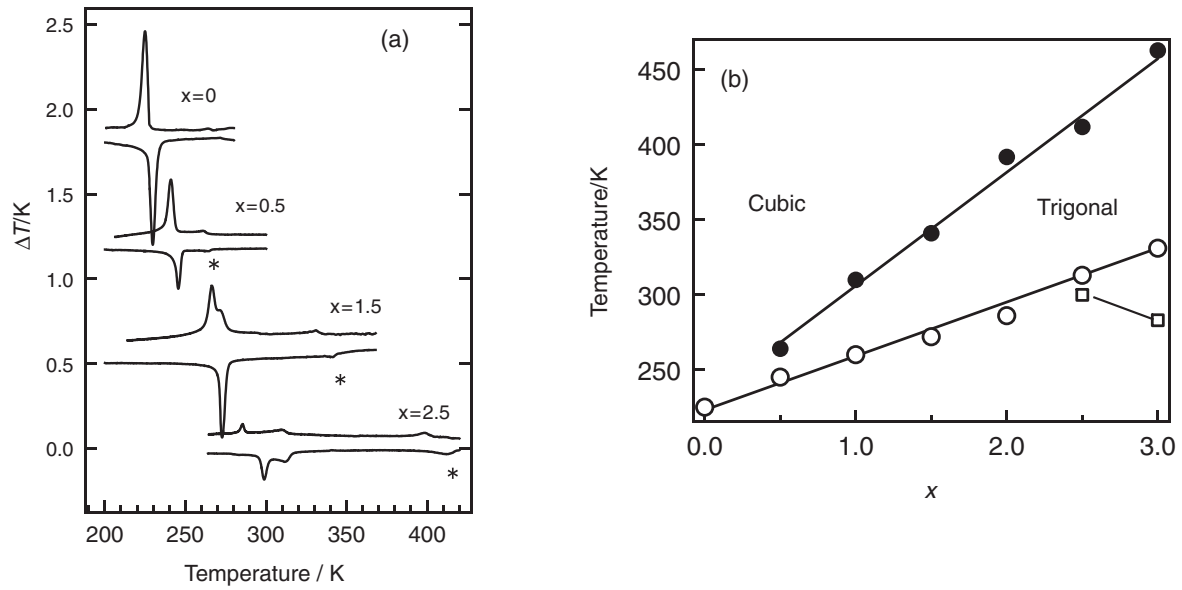

Figure 2. (a) DTA curves between 200–450 K for a series of $CH_3NH_3SnBr_{3-x}Cl_x$. Weak peaks denoted by * were assigned to the phase transitions from the trigonal to the cubic phases. (b) Phase diagram of $CH_3NH_3SnBr_{3-x}Cl_x$ determined by DTA and powder X-ray diffraction. □ denotes successive phase transitions from a triclinic to a monoclinic phase reported for $CH_3NH_3SnCl_3$.[10]

$CH_3NH_3SnBr_3$–$CH_3NH_3SnCl_3$, $CH_3NH_3SnBr_3$–$CH_3NH_3SnI_3$, and $CH_3NH_3SnI_3$–$CH_3NH_3SnCl_3$. The phase diagrams of the solid solutions as a function of the composite and the temperature were examined by means of DTA, X-ray diffraction, and ^{1}H NMR. Furthermore, in order to understand the characteristic band structure qualitatively, a simple tight-binding approach was applied to the one-dimensional –Sn–X– chain. The analytical expression was compared with previous theoretical investigations for the related perovskite halides.[17–21]

Experimental

Sample Preparation. Crude anhydride SnX_2 (X = Cl or Br) was directly synthesized from metallic Sn and hydrochloric or hydrobromic acid and the solution was successively evaporated to dryness. Crude SnX_2 was purified further by the Bridgman method as a single crystal. SnI_2 was synthesized as the precipitation from an aqueous solution of KI and $SnCl_2$. Although title solid solutions could be prepared from the relevant solutions, all samples were synthesized by solid-state reactions (ca. 180 °C) in order to control their compositions. The heating and grinding procedures were repeated several times until uniform solid-solutions were obtained.

Characterization. Samples were characterized by a powder X-ray diffractometer (Bruker D8) and further characterized by the successive Rietveld analysis (RIETAN).[23] Temperature dependence of the X-ray diffraction was performed by a Rad-B system equipped with a homemade high-temperature attachment. DTA measurement was performed using a homemade heat-flow-type DSC at a heating and cooling rate of 2 K min^{-1}, where ca. 100 mg of sample was sealed in a glass tube in order to avoid oxidation. Broadline ^{1}H NMR measurements as a function of temperature (100–400 K) were performed using a homemade automated apparatus operating at 6.37 T (Larmor frequency: 271.2 MHz).

Results and Discussion

DTA and X-ray Diffraction on $CH_3NH_3SnBr_{3-x}Cl_x$. Similar to the precipitations from the solution (Figure 1), a series of continuous solid solutions was confirmed between $CH_3NH_3SnBr_3$–$CH_3NH_3SnCl_3$, where continuous color changes were observed for the powder samples. However, the crystal system at 298 K changes from a cubic to a trigonal system above $x = 1.0$. In order to understand the phase diagram as a function of temperature and composition x, DTA measurements were performed in the temperature range between 200 and 400 K. Figure 2a shows some selective DTA curves for these solid solutions. Except $x = 0$, DTA curves show a common feature, i.e., a strong exothermic peak (200–300 K) and a weak one (denoted by *) at the higher temperature side. Above $x = 2.5$ the strong exothermic peak splits into two peaks which were assigned to the successive phase transitions reported for $x = 3.0$.[10] Figure 2b plots these peak temperatures against x. Figure 3 plots XRD patterns at 298 K for samples with $x = 0$, 1, 2, and 3, where a trigonal distortion is seen clearly for samples above $x = 1$. A representative Rietveld refinement plot at $x = 1.5$ is shown in Figure 4. The crystallographic parameters for a series of solid solutions and the structural parameters at $x = 1.5$ are summarized in Tables 1 and 2, respectively. The trigonal distortion at RT increases with x as shown in Figure 5. The resultant phase diagram determined by the DTA and X-ray measurements is summarized in Figure 2b as a function of x and temperature. Except for pure $CH_3NH_3SnBr_3$, a trigonal phase appears just below the respective cubic phase.

In order to investigate the relationship between phase transition and cation dynamics, broadline ^{1}H NMR was measured as a function of temperature. Figure 6 shows the temperature dependence of the FWHM line width, where line width transitions are observed at ca. 220 and 260 K for

Table 1. Crystallographic Data for $CH_3NH_3SnBr_{3-x}Cl_x$ at 298 K

	x					
	0	0.5	1.0	1.5	2.0	3.0[a)]
Crystal system	Cubic	Cubic	Trigonal	Trigonal	Trigonal	Trigonal
Space group	*Pm*3*m* (#221)	*Pm*3*m* (#221)	*R*3*m* (#160)	*R*3*m* (#160)	*R*3*m* (#160)	*R*3*m* (#160)
a/Å	5.901(1)	5.878(1)	5.855(1)	5.839(1)	5.799(1)	5.734
α/°	—	—	90.49(1)	91.16(1)	91.39(1)	91.9
R_F	0.060	0.062	0.063	0.065	0.083	
R_P	0.094	0.105	0.120	0.078	0.091	

a) $T = 360$ K, Ref. 10.

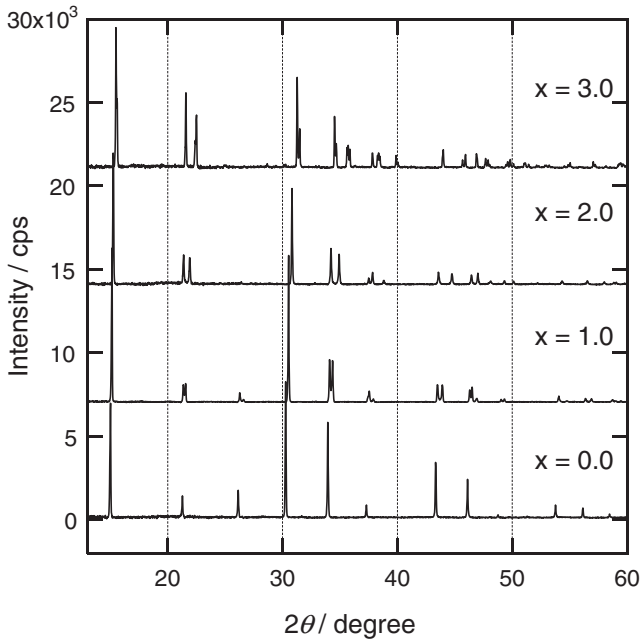

Figure 3. X-ray diffraction patterns for $CH_3NH_3SnBr_{3-x}Cl_x$ ($x = 0$, 1, 2, and 3).

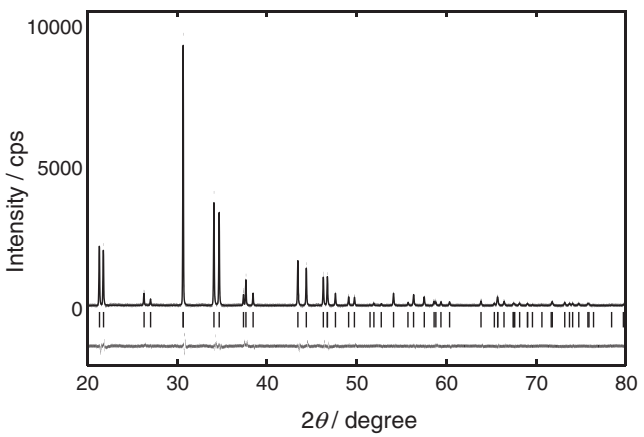

Figure 4. Typical example of the Rietveld analysis on the trigonal $CH_3NH_3SnBr_{1.5}Cl_{1.5}$ at 298 K.

Table 2. Structural Parameters for $CH_3NH_3SnBr_{1.5}Cl_{1.5}$ at 298 K

Atom/Unit	Point sym.	x	y	z	B_{eq}/Å^2
CH_3NH_3[a)]	3	−0.010(7)	$=x$	$=x$	48(1)
Sn	3	0.5	0.5	0.5	3.3(1)
Br/Cl	1	0.4778(9)	$=x$	−0.0059(14)	11.5(2)

a) Isoelectronic K^+ was used as a dummy.

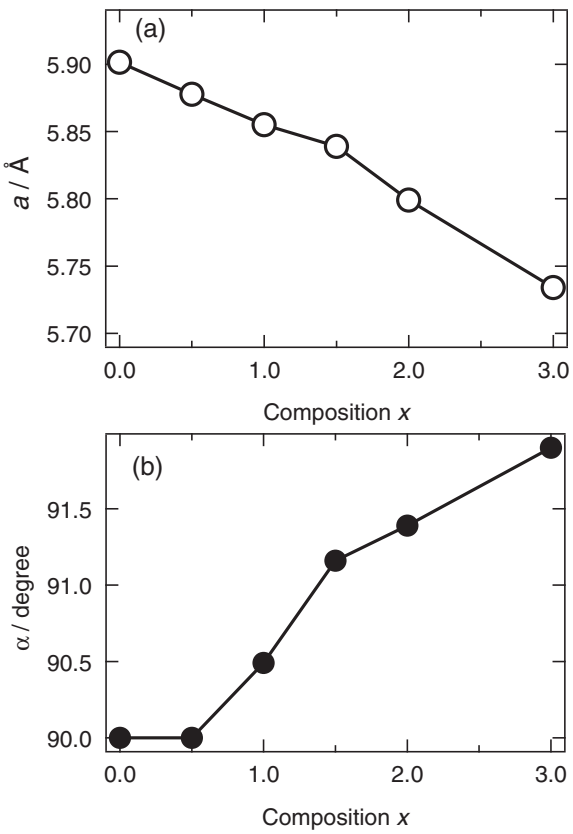

Figure 5. Composition dependence of the (a) trigonal lattice constant and (b) angle at 298 K. The trigonal lattice parameters for $CH_3NH_3SnCl_3$ at 360 K are shown together.

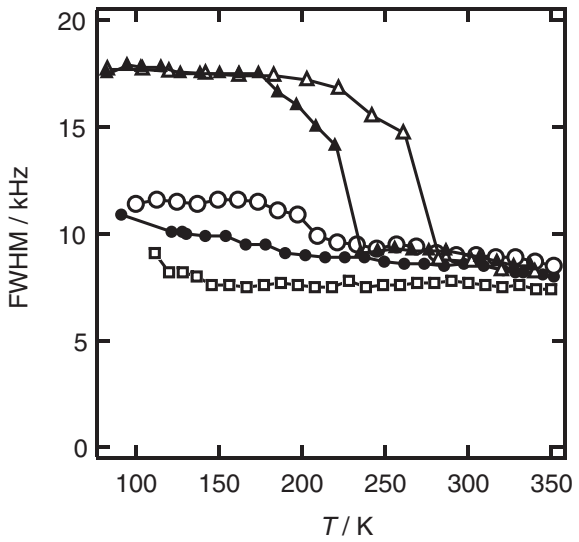

Figure 6. Temperature dependence of the broadline ^{1}H NMR FWHM line width as a function of temperature. ▲: $CH_3NH_3SnBr_3$, △: $CH_3NH_3SnBr_{1.5}Cl_{1.5}$, ○: $CH_3NH_3SnBr_2I$, ●: $CH_3NH_3SnBrI_2$, □: $CH_3NH_3SnI_3$.

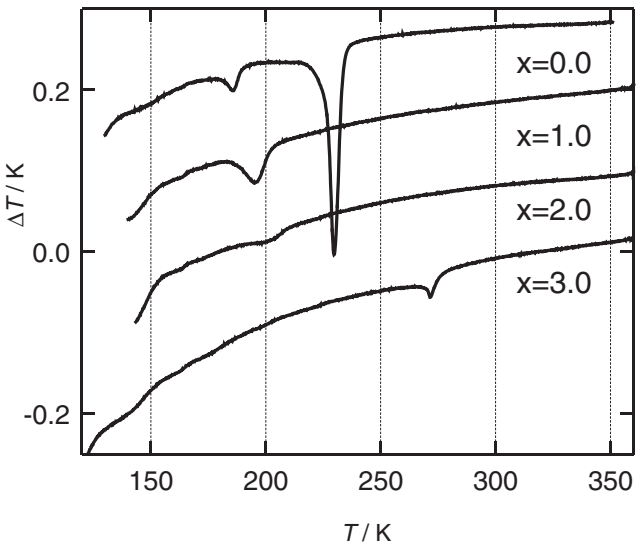

Figure 8. DTA curves for a series of $CH_3NH_3SnBr_{3-x}I_x$ ($x = 0$, 1, 2, and 3).

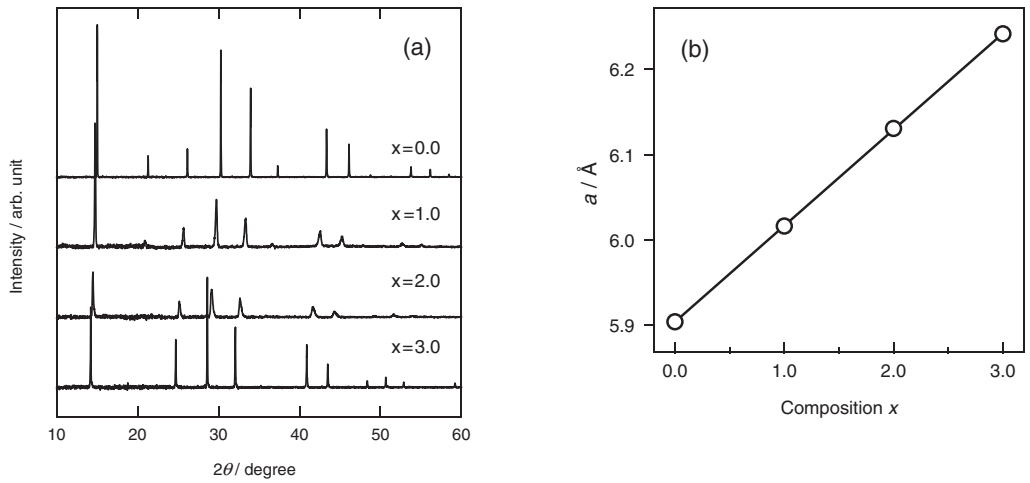

Figure 7. (a) X-ray diffraction patterns for $CH_3NH_3SnBr_{3-x}I_x$ ($x = 0$, 1, 2, and 3) and (b) cubic lattice constant against x. $a = 5.901(1)$, 6.016(1), 6.130(1), and 6.241(1) Å for $x = 0$, 1, 2, and 3, respectively.

$CH_3NH_3SnBr_3$ and $CH_3NH_3SnBr_{1.5}Cl_{1.5}$, respectively. According to the previous report on $CH_3NH_3SnBr_3$, ^{1}H NMR line width of about 17 kHz (4.25 G) corresponds to the partly averaged dipole–dipole interactions as a result of an axial reorientation of the cation around C–N axis, whereas the FWHM line width of about 9 kHz (2.1 G) suggests an isotropic reorientation of the whole $CH_3NH_3^+$ cation.[6] These line width transition temperatures agree well with the corresponding phase transitions. Therefore, the strong DTA peak is assigned to the onset of the isotropic orientational disorder of the cation. On the other hand, the weak one is assigned to the displacement transition from a slightly distorted trigonal to a cubic system, at which no color changes were observed.

According to a recent structural study on $CH_3NH_3SnBr_3$ at 215 K, strong ferroelectric distortion of the $SnBr_6$ octahedra was suggested from the synchrotron powder diffraction data.[12] The strong distortions of the $SnBr_6$ octahedra were suggested from the characteristic color change from red to yellow ($T_{tr} = 228$ K) and also from the ^{81}Br NQR spectrum which reflected the Sn–Br bonding character directly.[6]

DTA and X-ray Diffraction on $CH_3NH_3SnBr_{3-x}I_x$. Figure 7a shows X-ray diffraction patterns for a series of $CH_3NH_3SnBr_{3-x}I_x$ solid solutions. Continuous solid solution maintaining a cubic system was confirmed including end members. However, the diffraction peaks of the solid solutions were weaker and broader than those of the end-members, suggesting the poor crystallinity of the solid solution. The lattice constant increases linearly as a function of x as shown in Figure 7b. As Figure 8 shows, DTA behaviors are quite different from those of the $CH_3NH_3SnBr_{3-x}Cl_x$, i.e., strong exothermic peaks could not be detected between 150 and 350 K except pure $CH_3NH_3SnBr_3$. This means that the isotropic

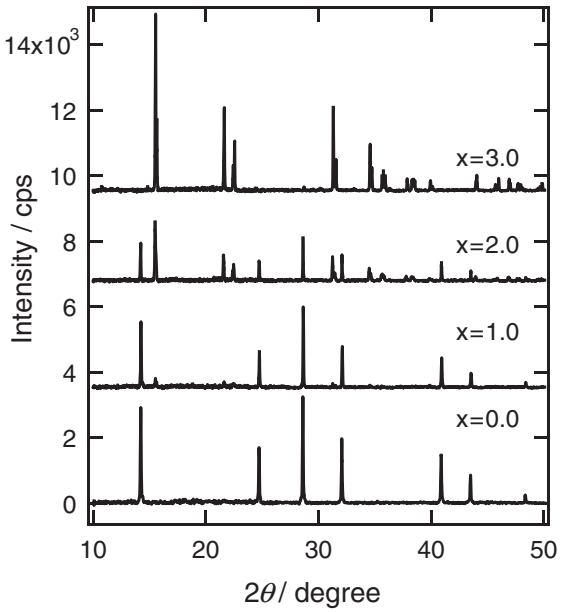

Figure 9. X-ray diffraction patterns for $CH_3NH_3SnI_{3-x}Cl_x$ ($x = 0$, 1, 2, and 3). Diffraction patterns for $x = 1$ and 2 are superpositions of the end members.

reorientation of the $CH_3NH_3^+$ does not freeze even at 150 K, probably because of the expansion of the anionic sublattice. In order to confirm the cation dynamics, FWHM of the ^{1}H NMR was observed as a function of temperature. As Figure 6 shows, an isotropic reorientation of the cation was confirmed even at 150 K for $CH_3NH_3SnI_3$. There is no clear line width transition for $x = 1$ or 2, however, it increases continuously below 220 K. These findings suggest that the onset temperature of the isotropic reorientation of the cation decreases with increasing the anionic sublattice and that the motion of the cation is not uniform throughout the solid solution.

According to our preliminary X-ray diffraction measurement on $CH_3NH_3SnI_3$ at 116 K, it belongs to a tetragonal system (space group: $I4/mcm$ with $a = 8.723(2)$ Å and $b = 12.471(2)$ Å), where the tilting of SnI_6 octahedra appears along the a axis and also in the bc plane. Therefore, the weak endothermic peaks at 271 ($x = 3.0$) and 201 K ($x = 2.0$) could be assigned to the phase transition from a cubic to a tetragonal phase having a displacement character. Whereas the endothermic peak at 195 K for $x = 1$ has some order–disorder character of the cation because ^{1}H NMR FWHM increases slightly at the same temperature stated above.

X-ray Diffraction on $CH_3NH_3SnI_{3-x}Cl_x$. The possibility of the solid solutions between chloride and iodide was also examined. As Figure 9 shows, the diffraction patterns for $x = 1$ and 2 are superpositions of the end members. Therefore, continuous solid solutions $CH_3NH_3SnI_{3-x}Cl_x$ could not be formed because of the large difference of the ionic radius, $r_I/r_{Cl} = 1.234$.

Dispersion Behavior of the One-Dimensional Energy Bond. The characteristic crystal properties of the ABX_3 perovskite, such as electronic conductivity or visible-light absorption, are strongly related to the electronic band structure of the perovskite in which infinite linear chains –B–X–B–X– are formed three-dimensionally. Many theoretical investigations on these Sn(II) perovskite halides have been reported and these calculations suggested that these halides are direct band gap semiconductors.[17,18,20,21]

If π-type overlaps and any interaction between s orbitals are neglected, the energy dependence of the cubic perovskite on the wavenumber (k) is given by just the sum of the three orthogonal directions, because three Sn 5p orbitals are orthogonal to each other. Therefore, one-dimensional analytical expression does not lose the three-dimensional crystal property. We will discuss the dispersion behavior of the energy band for these compounds analytically using a one-dimensional tight-binding approach.

In the case of a one-dimensional infinite chain of carbon pπ orbitals or s orbitals, Hückel theory provides an analytical expression for the energy of the orbitals. The energy of the j-th level e_j, for an N atoms chain is expressed as,[24]

$$e_j = \alpha + 2\beta \cdot \cos\frac{j\pi}{N+1} \tag{1}$$

Where α and β are energies of the atomic orbital and interaction between two adjacent orbitals, respectively. The lowest and highest levels will lie at $e = \alpha + 2\beta$ and $\alpha - 2\beta$ (α, $\beta < 0$), respectively. Between them orbitals lie continuously and hence form a band with the energy spread of $|4\beta|$. If each atomic orbital has one electron, a half-filled band is formed and hence an infinite chain of the atomic orbitals should be metallic. On the other hand, when an infinite chain of pσ orbitals between Sn(II) and halogen is formed, a little different situation occurs. As described before, we assumed that only 5p orbitals of the Sn could be utilized for the bonding. Then, each 5p orbital can form X–Sn–X bonds with the adjacent halogens, which could be regarded as a three-center-four-electron bond (3c-4e) found in a linear I_3^- anion.[25,26] We will discuss the case where there is no distortion, i.e., in the case of equally spaced –Sn–X–Sn–X– linear chains formed in the cubic lattice.

We introduce Bloch functions for the repeated unit of the Sn pσ and halogen pσ orbitals according to the text book of Albright,[24]

$$\begin{aligned}\phi_{Sn}(k) &= \frac{1}{\sqrt{N}}\Big[\ldots + \chi_{Sn}(r+a)\exp(-ika) \\ &\quad + \chi_{Sn}(r) + \chi_{Sn}(r-a)\exp(ika) + \ldots\Big] \\ \phi_X(k) &= \frac{1}{\sqrt{N}}\Big[\ldots + \chi_X\Big(r+\frac{a}{2}\Big)\exp\Big(-ik\frac{a}{2}\Big) \\ &\quad + \chi_X\Big(r-\frac{a}{2}\Big)\exp\Big(ik\frac{a}{2}\Big) + \ldots\Big]\end{aligned} \tag{2}$$

where a is a unit translation along a bond, i.e., $a/2$ corresponds to the Sn–X bond length, k is a wavenumber ($-\pi/a < k < \pi/a$), χ_{Sn} and χ_X are atomic pσ orbitals. In the Hückel approximation, the energies of atomic $\phi_{Sn}(k)$ and $\phi_X(k)$ orbitals are defined as follows:

$$\begin{aligned}H_{11}(k) &= \langle\chi_{Sn}|H|\chi_{Sn}\rangle = \alpha_{Sn} \\ H_{22}(k) &= \langle\chi_X|H|\chi_X\rangle = \alpha_X\end{aligned} \tag{3}$$

Nondiagonal element $H_{12}(k)$ contains nearest neighbor interactions and is reduced to,

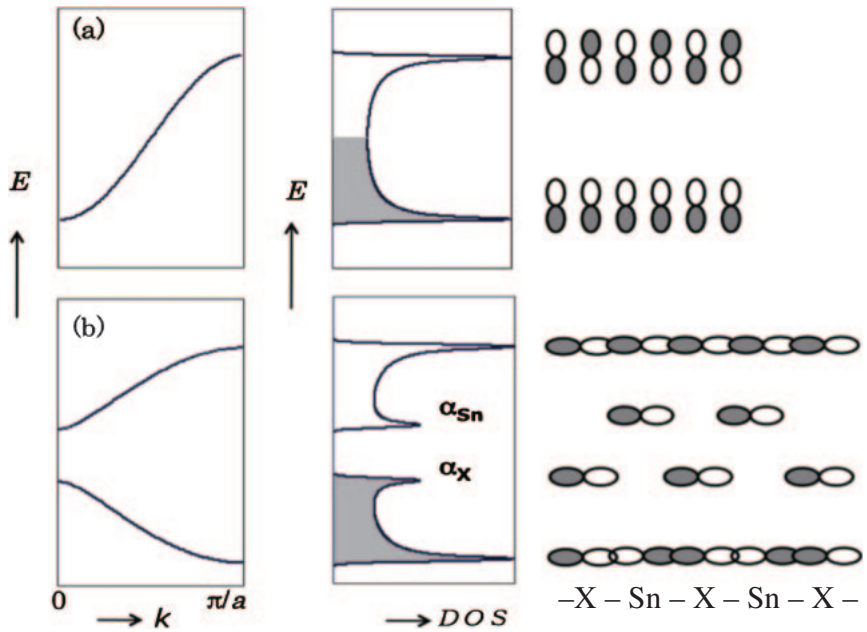

Figure 10. Schematic representations of the dispersion behavior, density of state (DOS) and the form of the wave functions for one-dimensional chain. (a) An infinite chain formed by the overlap of adjacent pπ orbitals and (b) one-dimensional –Sn–X– chain, in which the bond is formed by the overlap of adjacent pσ orbitals.

$$H_{12}(k) = \langle \chi_{Sn}|H|\chi_X\rangle = 2\beta \sin\left(\frac{ka}{2}\right) \quad (4)$$

It should be noted that the bonding interaction is formed at $k = \pi/a$ and the antibonding interaction at $k = 0$, in contrast to the linear chain of the pπ or s orbitals. Then the secular determinant becomes:

$$\begin{vmatrix} \alpha_{Sn} - e(k) & 2\beta \sin\dfrac{ka}{2} \\ 2\beta \sin\dfrac{ka}{2} & a_X - e(k) \end{vmatrix} = 0 \quad (5)$$

Solution of the determinant leads to,

$$E = \alpha_{Sn} \text{ and } \alpha_X \text{ for } k = 0 \quad (6)$$

and

$$E = \frac{(\alpha_{Sn} + \alpha_I) \pm \sqrt{(\alpha_{Sn} + \alpha_I)^2 - 4(\alpha_{Sn}\alpha_I - 4\beta^2)}}{2} \quad (7)$$

for $k = \pi/a$. Therefore, the dispersion behavior of the energies as a function of k is shown in Figure 10 together with the corresponding DOS in a schematic fashion. There is a nondegenerate integration between levels α_{Sn} and α_I. Since the infinite –Sn–X– chain contains N electrons, the lower band is fully occupied and the upper band is empty. Figure 10 shows clearly that the perovskite halides of Sn(II) should be a direct band gap ($E_g = |\alpha_{Sn} - \alpha_X|$) semiconductor at $k = 0$. Since the band gap is expected to increases in the order of $|\alpha_{Sn} - \alpha_I| < |\alpha_{Sn} - \alpha_{Br}| < |\alpha_{Sn} - \alpha_{Cl}|$ from their electronegativities, the color change of the perovskite could be easily understandable. According to the theoretical calculations for these Sn(II) perovskite halides, a direct band gap was reported at the Γ point,[17] which corresponds to the $k = 0$ in our one-dimensional model. Furthermore, theoretical calculations suggested that the top of the valence band is mainly dominated by halogen p-orbitals and the bottom of the conduction band is essentially dominated by Sn p-orbitals. These results are also consistent with our expression shown in Figure 10. Recently, Chiarella et al. reported band gap energies (E_g) to be 2.15 and 3.69 eV for $CH_3NH_3SnBr_3$ and $CH_3NH_3SnCl_3$, respectively, from the optical measurements using thin firms.[17] They also computed E_g from the theoretical investigation to be 1.90 and 3.44 eV for these two compounds. The continuous color change of the solid solutions $CH_3NH_3SnBr_{3-x}Cl_x$ could be understandable similarly. It is interesting to note that the characteristic color change below 228 K for $CH_3NH_3SnBr_3$ is mainly attributed to the Peiels type distortion appearing in the equally-spaced –Sn–Br–Sn–Br– chain.

Conclusion

Tunable semiconductors could be prepared as solid solutions, $CH_3NH_3SnBr_{3-x}Cl_x$ and $CH_3NH_3SnBr_{3-x}I_x$, which were characterized by DTA, X-ray diffraction, and ^{1}H NMR. In the former perovskite solid solution, the crystal color changes from a red to a colorless state with increasing x, although a slight trigonal distortion appears at 298 K ($x \geq 1.0$). On the other hand, solid solution $CH_3NH_3SnBr_{3-x}I_x$ forms cubic perovskite with a black color over the whole x region. The characteristic color and the semiconducting properties of these perovskites could be qualitatively understandable using an analytical expression based on a one-dimensional tight-binding approach.

This work was partly supported by a Grant-in-Aid for Scientific Research (No. 22550126) from the Japan Society for the Promotion of Science (JSPS) and also partly supported by the "Strategic Research Base Development" Program for Private Universities subsidized by MEXT (2009) (No. S0901022).

References

1 C. Li, X. Lu, W. Ding, L. Feng, Y. Gao, Z. Guo, *Acta Crystallogr., Sect. B* **2008**, *64*, 702.

2 V. Manivannan, P. Parhi, J. W. Kramer, *Bull. Mater. Sci.* **2008**, *31*, 987.

3 S. Mahlik, K. Wiśniewski, M. Grinberg, H. J. Seo, *Opt. Mater.* **2011**, *33*, 996.

4 P. Berastegui, S. Hull, S.-G. Eriksson, *J. Phys.: Condens. Matter* **2001**, *13*, 5077.

5 Y. Yamane, K. Yamada, K. Inoue, *Solid State Ionics* **2008**, *179*, 605.

6 K. Yamada, S. Nose, T. Umehara, T. Okuda, S. Ichiba, *Bull. Chem. Soc. Jpn.* **1988**, *61*, 4265.

7 K. Yamada, S. Funabiki, H. Horimoto, T. Matsui, T. Okuda, S. Ichiba, *Chem. Lett.* **1991**, 801.

8 K. Yamada, T. Matsui, T. Tsuritani, T. Okuda, S. Ichiba, *Z. Naturforsch., A: Phys. Sci.* **1990**, *45*, 307.

9 N. Onoda-Yamamuro, T. Matsuo, H. Suga, *J. Chem. Thermodyn.* **1991**, *23*, 987.

10 K. Yamada, Y. Kuranaga, K. Ueda, S. Goto, T. Okuda, Y. Furukawa, *Bull. Chem. Soc. Jpn.* **1998**, *71*, 127.

11 Y. Lee, D. B. Mitzi, P. W. Barnes, T. Vogt, *Phys. Rev. B* **2003**, *68*, 020103(R).

12 I. Swainson, L. Chi, J.-H. Her, L. Cranswick, P. Stephens, B. Winkler, D. J. Wilson, V. Milman, *Acta Crystallogr., Sect. B* **2010**, *66*, 422.

13 D. B. Mitzi, C. A. Feild, Z. Schlesinger, R. B. Laibowitz, *J. Solid State Chem.* **1995**, *114*, 159.

14 D. B. Mitzi, K. Liang, *J. Solid State Chem.* **1997**, *134*, 376.

15 F. Chiarella, P. Ferro, F. Licci, M. Barra, M. Biasiucci, A. Cassinese, R. Vaglio, *Appl. Phys. A: Mater. Sci. Process.* **2007**, *86*, 89.

16 T. Matsushima, K. Fujita, T. Tsutsui, *Jpn. J. Appl. Phys.* **2006**, *45*, 523.

17 F. Chiarella, A. Zappettini, F. Licci, I. Borriello, G. Cantele, D. Ninno, A. Cassinese, R. Vaglio, *Phys. Rev. B* **2008**, *77*, 045129.

18 K. Shum, Z. Chen, J. Qureshi, C. Yu, J. J. Wang, W. Pfenninger, N. Vockic, J. Midgley, J. T. Kenney, *Appl. Phys. Lett.* **2010**, *96*, 221903.

19 D. E. Parry, M. J. Tricker, J. D. Donaldson, *J. Solid State Chem.* **1979**, *28*, 401.

20 S. K. Bose, S. Satpathy, O. Jepsen, *Phys. Rev. B* **1993**, *47*, 4276.

21 I. Borriello, G. Cantele, D. Ninno, *Phys. Rev. B* **2008**, *77*, 235214.

22 A. Kojima, K. Teshima, Y. Shirai, T. Miyasaka, *J. Am. Chem. Soc.* **2009**, *131*, 6050.

23 F. Izumi, T. Ikeda, *Mater. Sci. Forum* **2000**, *321–324*, 198.

24 T. A. Albright, J. K. Burdett, M.-H. Whangbo, *Orbital Interactions in Chemistry*, John Wiley & Sons, **1985**, Chap. 13.

25 K. Yamada, T. Okuda, in *Chemistry of Hypervalent Compounds*, ed. by K.-y. Akiba, Wiley-VCH, New York, **1995**, Chap. 3, pp. 49–80.

26 G. C. Pimentel, R. D. Spratley, in *Chemical Bonding Clarified through Quantum Mechanics*, Holden-Day, Inc., **1969**, Chap. 7.